LETTER

https://doi.org/10.1038/s41586-018-0520-5

A cortical filter that learns to suppress the acoustic consequences of movement

David M. Schneider[1,2,3], Janani Sundararajan[1,3] & Richard Mooney[1]*

Sounds can arise from the environment and also predictably from many of our own movements, such as vocalizing, walking, or playing music. The capacity to anticipate these movement-related (reafferent) sounds and distinguish them from environmental sounds is essential for normal hearing[1,2], but the neural circuits that learn to anticipate the often arbitrary and changeable sounds that result from our movements remain largely unknown. Here we developed an acoustic virtual reality (aVR) system in which a mouse learned to associate a novel sound with its locomotor movements, allowing us to identify the neural circuit mechanisms that learn to suppress reafferent sounds and to probe the behavioural consequences of this predictable sensorimotor experience. We found that aVR experience gradually and selectively suppressed auditory cortical responses to the reafferent frequency, in part by strengthening motor cortical activation of auditory cortical inhibitory neurons that respond to the reafferent tone. This plasticity is behaviourally adaptive, as aVR-experienced mice showed an enhanced ability to detect non-reafferent tones during movement. Together, these findings describe a dynamic sensory filter that involves motor cortical inputs to the auditory cortex that can be shaped by experience to selectively suppress the predictable acoustic consequences of movement.

Auditory activity in the brains of humans and other mammals is suppressed during a wide variety of movements, including vocalization and locomotion[1,3–9]. Although the stereotyped and often simple acoustic consequences (that is, auditory reafference) of rhythmic movements such as licking or chewing can be suppressed by brainstem mechanisms[8], a more flexible form of movement-related suppression is

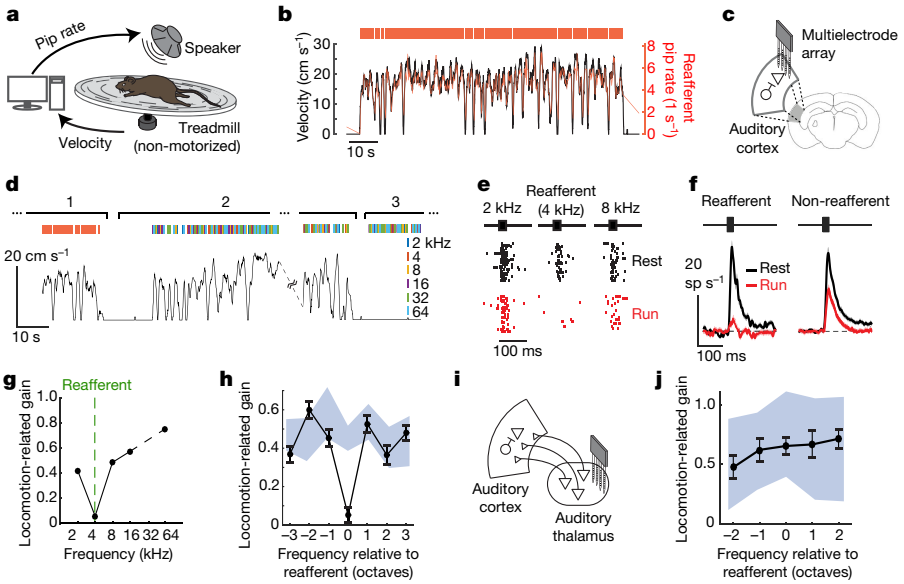

Fig. 1 | Locomotion-related suppression is specific for the frequency of self-generated sounds. a, Mice were acclimated to a closed-loop acoustic virtual reality (aVR) system. **b**, Example traces of locomotion (black trace), timing of individual aVR tone pips (red ticks), and instantaneous rate of aVR tone pips (red trace). **c**, Extracellular recordings were made from auditory cortical neurons during running and resting. The mouse brain in this figure has been reproduced with permission[27]. **d**, During electrophysiology, mice first heard the reafferent tone frequency that they expected treadmill running to produce (for example, 4 kHz) (phase 1). During phase 2, mice heard tones that were yoked in time to their running speed but with random frequency. During phase 3, mice heard tones of random frequency while at rest. **e**. Action potential responses from an example neuron while at rest (black, phase 3 from **d**) and while running (red, phase 2 from **d**) following playback of the expected reafferent frequency (4 kHz) as well as tone frequencies one octave away. **f**, Population peri-stimulus-time histograms (PSTHs) showing neural responses to reafferent (left) and non-reafferent (right) frequencies during running (red) and resting (black) conditions. Responses to non-reafferent sounds are averaged across all five non-reafferent frequencies. During running, responses to the expected reafferent frequency were suppressed relative to non-reafferent frequencies ($N = 11$ mice, $n = 317$ neurons, $P = 1.1 \times 10^{-18}$). **g**, Locomotion-related suppression of an example auditory cortical neuron. **h**, Average locomotion-related suppression (black, mean ± s.e.) of auditory cortical neurons, centred on the expected reafferent frequency heard by each mouse ($N = 11$ mice, $n = 317$ neurons). Blue area shows 95% confidence bounds. **i**, Extracellular recordings were made from the auditory thalamus during running and resting following 6–9 days of aVR acclimation. **j**, Locomotion-related suppression (black, mean ± s.e.) of auditory thalamic neurons ($N = 5$ mice, $n = 109$ neurons) is not specific to the expected reafferent frequency. For statistical details, see Methods.

[1]Department of Neurobiology, Duke University School of Medicine, Durham, NC, USA. [2]Center for Neural Science, New York University, New York, NY, USA. [3]These authors contributed equally: David M. Schneider, Janani Sundararajan. *e-mail: mooney@neuro.duke.edu

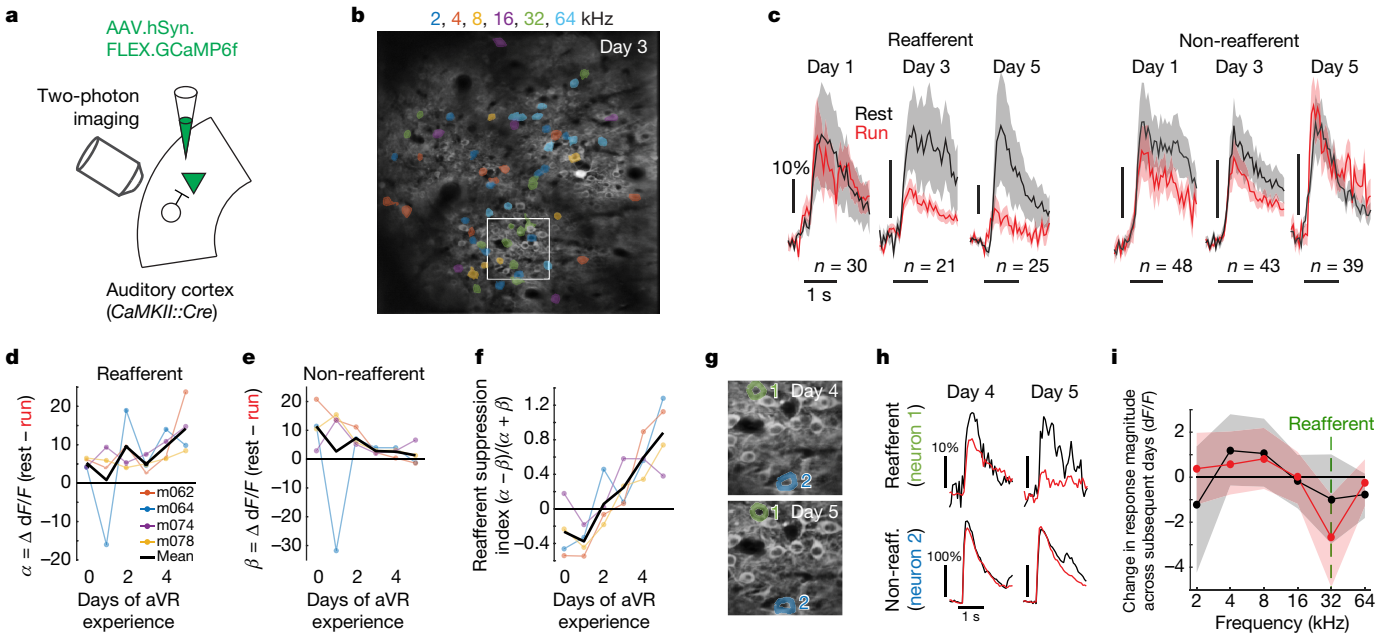

Fig. 2 | Reafferent suppression arises in parallel with sensory–motor experience. a, Injection of AAV encoding Cre-dependent GCaMP6f into auditory cortex of *CaMK2::Cre* mouse followed by calcium imaging of layer 2/3 excitatory neurons during aVR experience over several days. **b**, Maximum projection of an example field of layer 2/3 excitatory neurons in auditory cortex from a mouse acclimated to aVR experience producing 32-kHz tones. Colour represents the best frequency of every neuron. White box shows region in **g**. **c**, Population-averaged calcium transients evoked by the expected reafferent frequency (left) and a non-reafferent frequency (right, two octaves away) during rest (black) and running (red) following 1, 3 and 5 days of aVR experience. Shaded areas show mean ± s.e. **d**, Magnitude of locomotion-related suppression (α) for the expected reafferent frequency ($N = 4$ mice). **e**, Magnitude of locomotion-related suppression (β) for non-reafferent frequencies (two octaves lower). **f**, Selectivity of locomotion-related suppression for the expected reafferent frequency $[(\alpha - \beta)/(\alpha + \beta)]$. Values greater than zero indicate stronger locomotion-related suppression at the reafferent frequency; values less than zero indicate stronger locomotion-related suppression at non-reafferent frequencies. **g**, Maximum projection on subsequent days, zoomed in on the region outlined in white panel in **b**. **h**, Average calcium traces from two example neurons shown in **g** during days 4 and 5 of aVR experience. Responses for neuron 1 are to 32-kHz tones (the expected reafferent frequency) and responses for neuron 2 are to 2-kHz tones (a non-reafferent frequency). Black traces, rest; red traces, running. **i**, In two mice, 241 sound-responsive neurons were monitored across six pairs of subsequent days of aVR experience. Change in tuning curves across subsequent days (black, rest; red, running). Shaded regions are 95% confidence bounds. For statistical details, see Methods.

thought to arise independently in the auditory cortex through mechanisms that are not well understood[1,6,10–13]. To begin to identify these cortical mechanisms, we developed an acoustic virtual reality (aVR) system in which head-fixed mice on a treadmill heard a series of tones presented at a rate proportional to their running speed, simulating an experimentally adjustable yet predictable form of auditory reafference associated with locomotion (Fig. 1a, b; Extended Data Fig. 1a–d; Supplementary Video 1). After about a week of aVR experience, auditory cortical responses to the reafferent tone during locomotion were nearly abolished, whereas responses to frequencies one or more octaves distant from the reafferent frequency showed more modest suppression (similar to that seen during locomotion in aVR-naive mice[1]; Fig. 1c–f). Notably, this differential suppression manifested only during movement; in resting mice, a similar fraction of auditory cortical neurons responded to reafferent and non-reafferent tones, and they did so with equivalent firing rates (Fig. 1e, f and Extended Data Fig. 2a–d).

To further characterize the movement-dependent filter formed by aVR experience, we compared the frequency tuning curves of auditory cortical neurons at running and at rest and calculated a locomotion-related gain function for each neuron (Fig. 1g). Regardless of a neuron's best frequency, locomotion-related suppression was greater for the reafferent tone than for tones one or more octaves away, with tones half an octave from the reafferent frequency showing intermediate suppression during locomotion (Fig. 1h; Extended Data Figs. 2e–h, 3a). The width of this 'notch' filter may be constrained by the tuning widths of auditory cortical inhibitory neurons[14] and more broadly conforms to the idea that excitatory neurons in sensory cortex receive input from local inhibitory neurons tuned to both similar and dissimilar stimulus features[15,16]. Movement-related suppression in auditory thalamic neurons remained flat across sound frequencies (Fig. 1i, j), as previously observed in aVR-naive mice[1,4,17], and reafferent tones were more strongly suppressed in infragranular than supragranular auditory cortex (Extended Data Fig. 3b–d), indicating that circuits local to the auditory cortex are a likely source of the reafferent notch filter that arises following aVR experience.

The formation of this auditory cortical filter required a predictable and relatively prolonged association of movement with an ensuing sound. Mice acclimated for about a week on a treadmill in which fixed-frequency tones were presented only at rest did not display enhanced cortical suppression at the training frequency during rest or running (Extended Data Fig. 4a, b). Furthermore, mice acclimated for about a week on a treadmill in which tones were presented at a fixed tempo during locomotion regardless of running speed (that is, 'metronome'-experienced mice) showed no enhanced locomotion-related auditory cortical suppression at the training frequency (Extended Data Fig. 4c, d). Moreover, in aVR-experienced mice, enhanced suppression of the reafferent tone was evident as soon as they began to move on the treadmill, whereas stimulus-specific adaptation emerged more slowly and only after several tone presentations (that is, measured at the non-reafferent frequency; Extended Data Fig. 4e, f). Finally, one hour of aVR experience (around 1,000–3,000 reafferent tones) was not sufficient to induce any enhancement of locomotion-related suppression at the reafferent frequency (Extended Data Fig. 4g).

To determine more precisely the time course over which this notch filter arises, we used two-photon calcium methods to longitudinally image layer 2/3 excitatory neurons in the auditory cortex of mice across their first 5 days of aVR experience (Fig. 2a, b). Across days, tuning curves measured during rest were relatively stable ($r = 0.53$), but at

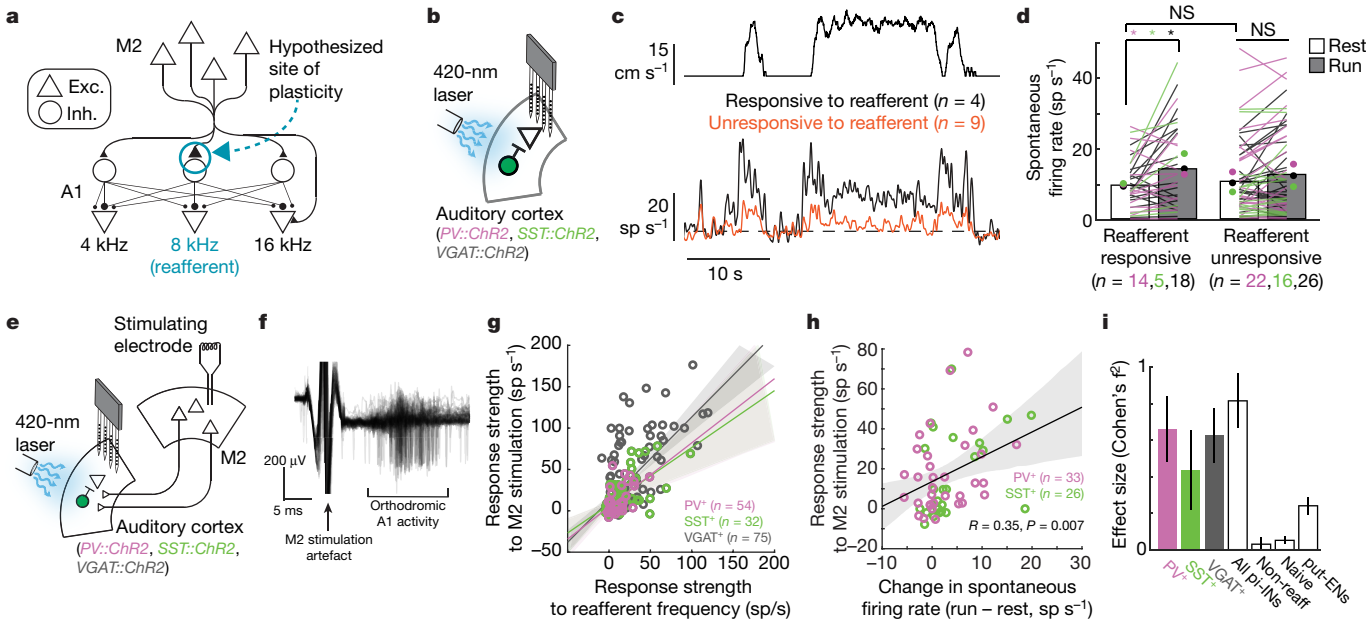

Fig. 3 | Reafferent-tuned inhibitory neurons increase their activity during locomotion and receive enhanced motor cortical input. **a**, Proposed model of experience-dependent strengthening of M2 inputs onto inhibitory neurons tuned to the reafferent frequency in the auditory cortex (blue circle). Synapse strength is proportional to size. **b**, Extracellular recording from photo-identified inhibitory neurons (pi-INs) in the auditory cortex. **c**, Top, locomotion velocity as a function of time. Bottom, spontaneous activity of simultaneously recorded pi-INs that were responsive to the reafferent frequency (black) or were not, but were responsive to other frequencies (orange). **d**, PV^+ (magenta), SST^+ (green) and $VGAT^+$ (black) pi-INs that are responsive to the reafferent frequency increase their firing rate significantly during locomotion, unlike pi-INs that are not responsive to the expected reafferent frequency ($^*P < 0.05$, Wilcoxon signed rank test). **e**, Extracellular recording from pi-INs in the auditory cortex. A bipolar microstimulating electrode was implanted in M2. **f**, Example of M2 stimulation-evoked action potentials recorded from a $VGAT^+$ pi-IN in auditory cortex. **g**, pi-INs that were more strongly driven by the reafferent frequency were more strongly recruited by electrical stimulation in M2. Solid lines and shadows show linear regression and 95% confidence bounds, respectively. **h**, Changes in spontaneous firing rate during locomotion relative to rest for pi-INs (PV^+ and SST^+) were significantly correlated with the magnitude of the same neurons' responses to M2 electrical stimulation. **i**, Effect size of the correlations shown in **g** and for four other conditions. All pi-INs: pi-INs from PV^+, SST^+ and $VGAT^+$ mice. Non-reaff: same neurons as shown in **g** ($VGAT^+$) but for responses to a non-reafferent tone. Naive: pi-INs from $VGAT^+$ mice that were acclimated to a quiet treadmill. put-ENs: putative excitatory neurons in auditory cortex of *VGAT::ChR2* mice acclimated to aVR. Error bars show 95% confidence bounds. For statistical details, see Methods.

the population level, locomotion-related suppression became progressively more specific for the reafferent frequency (Fig. 2c). The emergence of frequency-specific suppression during locomotion involved both increased suppression of the reafferent frequency and decreased suppression of non-reafferent frequencies (Fig. 2d–f). Tracking the activity of a subset of the same neurons ($n = 241$ from two mice) across consecutive days of aVR experience revealed that their tuning curves measured during locomotion—but not during rest—changed only at the reafferent frequency, with individual neurons becoming less responsive across consecutive days (Fig. 2g–i).

Auditory cortical interneurons integrate auditory inputs with locomotor-related signals from the secondary motor cortex (M2)[1,18,19] and form inhibitory synapses on both similarly and dissimilarly tuned excitatory cells, affording a substrate on which aVR experience could act to sculpt the movement-dependent notch filter described here[1,18] (Fig. 3a). To explore this possibility, we expressed channelrhodopsin (ChR2) in genetically identified inhibitory neurons (parvalbumin $(PV)^+$ (encoded by *PV* (also known as *Pvalb*)), somatostatin $(SST)^+$, or vesicular γ-aminobutyric acid (GABA) transporter $(VGAT)^+$ (encoded by *VGAT* (also known as *Slc32a1*)) neurons; see Methods), acclimated mice to aVR experience for about a week, and then recorded the action potential activity of photo-identified auditory cortical inhibitory cells (Fig. 3b and Extended Data Fig. 5a, b). During running, the spontaneous firing rates in only those inhibitory neurons responsive to the reafferent frequency increased, while their responses to reafferent and non-reafferent tones decreased modestly (Fig. 3c, d; Extended Data Fig. 5c). By contrast, the spontaneous firing rates of putative excitatory neurons decreased slightly during locomotion (Extended Data Fig. 5d). Moreover, the magnitude of the running-related increase in an inhibitory neuron's spontaneous firing rate scaled with the strength of its response to the reafferent frequency (Extended Data Fig. 5e). Finally, locomotion-related suppression at the reafferent frequency comprised both divisive and subtractive components, consistent with the involvement of both PV^+ and SST^+ interneurons[20] (Extended Data Fig. 5f). Therefore, aVR experience selectively enhanced the movement-dependent recruitment of inhibitory interneurons that respond to the reafferent frequency.

One idea is that aVR experience strengthens the connections between M2 and auditory cortical interneurons that respond to the reafferent frequency, resulting in their selective recruitment during locomotion. To test this idea, we calculated frequency-tuning curves of photo-identified PV^+, SST^+ and $VGAT^+$ inhibitory neurons in the auditory cortex of aVR-experienced mice. We then applied brief current pulses in M2 and measured the resulting action potential activity in these identified interneurons (Fig. 3e, f). Auditory cortical inhibitory neurons that responded strongly to the reafferent frequency were driven more strongly by M2 stimulation than were inhibitory neurons that responded only weakly or not at all to the reafferent frequency (Fig. 3g, i and Extended Data Fig. 5g, j). Moreover, the PV^+ and SST^+ inhibitory neurons that were activated most strongly by M2 stimulation in resting mice showed the greatest increases in spontaneous firing rates when the mouse was running (Fig. 3h). Using a similar approach, we also detected a similar but weaker correlation for auditory cortical excitatory neurons in aVR-experienced mice (Fig. 3i and Extended Data Fig. 5h, j). These differential effects of M2 stimulation on auditory cortical excitatory and inhibitory neurons are consistent with the observation that M2 synapses excite both cell types but exert a primarily suppressive effect on auditory cortical activity through feedforward

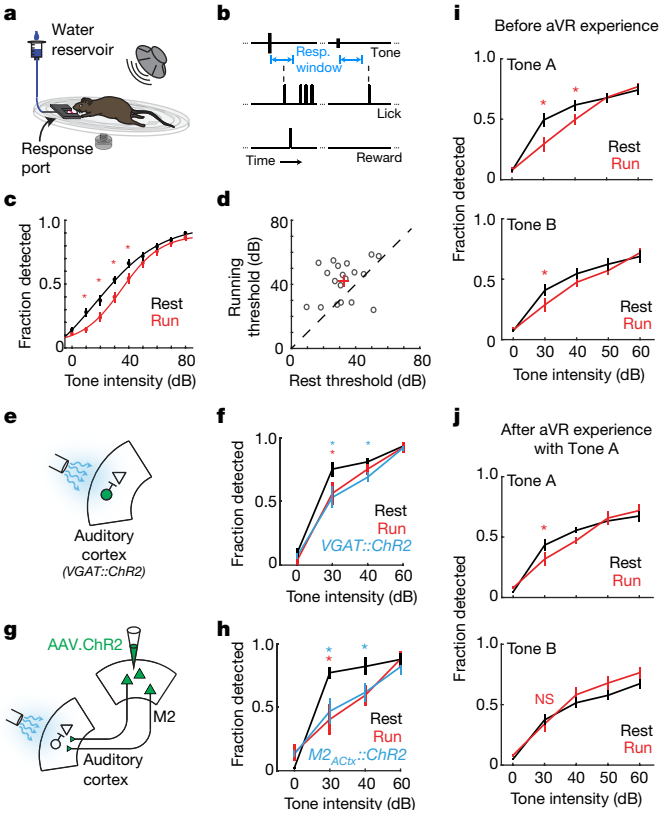

Fig. 4 | Tone detection behaviour is compromised by locomotion, is auditory-cortex dependent, and adapts following aVR experience. **a**, Mice were trained to lick a response port upon hearing a tone while resting or running on a treadmill. **b**, Tones were presented with random inter-tone intervals following a period without spontaneous licking. Mice were rewarded for licking within 1 s of tone presentation. **c**, Average psychometric functions showing detection rates as a function of tone intensity while mice were resting (black) or running (red). $N = 19$ mice, Red asterisk, $P < 0.005$. **d**, Behavioural threshold (intensity at 50% performance) during resting and running for each mouse (black circles; red plus denotes mean threshold). Dashed line shows unity. $N = 19$ mice, $P = 0.009$, paired t-test. **e**, Optogenetic activation of inhibitory neurons in auditory cortex during tone detection. **f**, Tone detection performance ($N = 4$ mice) during rest (black), running (red) and rest with optogenetic activation of auditory cortical inhibitory neurons (blue). Mice were worse at detecting tones during optogenetic trials compared to non-optogenetic trials at rest (blue asterisk, $P < 0.05$) and during running compared to rest (red asterisk, $P < 0.05$). **g**, Optogenetic activation of ChR2$^+$ M2 terminals in auditory cortex during tone detection. **h**, Tone detection performance ($N = 4$ mice) during rest (black), running (red) and rest with optogenetic activation of M2 terminals in auditory cortex (blue). Mice were worse at detecting tones during optogenetic trials compared to non-optogenetic trials at rest (blue asterisk, $P < 0.05$) and during running compared to rest (red asterisk, $P < 0.05$). **i**, Tone detection performance ($N = 10$ mice) during rest and running for naive mice performing a two-frequency detection task (red asterisk, $P < 0.05$). **j**, As in **i**, but following aVR experience with Tone A (red asterisk, $P < 0.05$). Error bars show s.e.m. For further statistical details, see Methods and Supplementary Table 1.

inhibition[1,18]. Finally, in aVR-naive mice, there was only a weak correlation between tone-evoked and M2-stimulation-evoked responses in auditory cortical interneurons (Fig. 3i and Extended Data Fig. 5i, j).

To investigate how movement-related signals in the auditory cortex influence auditory perception, we trained mice to detect tones while running and resting and confirmed that this tone detection task required auditory cortical activity (Fig. 4a, b; Supplementary Video 2; Extended Data Fig. 6a). This test revealed that mice were significantly worse at detecting tones at intermediate intensities (10–40 dB) while running than at rest, despite displaying equal levels of motivation in these two states (Fig. 4c, d; Extended Data Fig. 6b). Furthermore, optogenetic activation of inhibitory interneurons or M2 axon terminals in the auditory cortex degraded performance in resting mice at these intermediate sound intensities, indicating that the same circuit elements that are influenced by aVR experience modulate hearing in a movement-dependent manner (Fig. 4e–h; Extended Data Fig. 6c–f). By contrast, optogenetically activating inhibitory interneurons in visual cortex, illuminating GFP-expressing M2 terminals in the auditory cortex, or simply illuminating the intact skull in resting mice did not diminish their ability to detect tones (Extended Data Fig. 6g–i).

A remaining issue is whether the auditory cortical filter formed by aVR experience improves the mouse's ability to detect non-reafferent tones during movement, as hypothesized for brain mechanisms that suppress predictable sensory reafference[2,21,22]. We trained mice to detect two different tones (tones A and B, separated by two octaves), which were randomly interleaved from one trial to the next. After several days of training, mice showed a similar deficit in detecting both tones during locomotion, similar to mice trained on a single tone (Fig. 4i). Mice then received about a week of aVR experience in which only one of the tones (tone A) was used as a reafferent training stimulus. Following aVR experience, mice no longer showed a locomotion-related deficit in detecting the non-reafferent tone (tone B), even though they continued to show a movement-related deficit in detecting the reafferent tone (tone A) (Fig. 4i, j). Therefore, aVR experience not only selectively suppresses auditory cortical responses to predictable reafferent sounds, but also improves the ability of mice to detect unpredicted sounds during movement (Extended Data Fig. 6j, k).

Our findings establish that temporally coupled locomotor–auditory experience results in the formation of a movement-dependent filter that suppresses auditory cortical responses to predictable self-generated sounds. A plausible idea is that coincident motor and auditory activity during sound-generating movements strengthens M2 synapses onto PV$^+$ and SST$^+$ interneurons, or onto neurons interposed between M2 and these auditory cortical interneurons, leading to enhanced movement-related suppression of auditory cortical responses to the reafferent tone[23] and an enhanced ability to detect non-reafferent tones during movement[24,25]. Notably, aVR experience also reduced locomotion-dependent suppression at non-reafferent frequencies in layer 2/3 of the auditory cortex, providing an auditory cortical correlate of this adaptive perceptual change. The involvement of M2 in this form of auditory cortical suppression is reminiscent of the motor cortex-mediated suppression of responses to predictable stimuli in mouse primary visual cortex[26], consistent with a generalized predictive cortical mechanism. Ultimately, the motor–auditory cortical circuit characterized here can flexibly encode the relationship between a movement and the sound it produces, helping to maintain sensitivity to novel sounds in the environment while also monitoring the acoustic consequences of sound-generating movements.

Online content

Any methods, additional references, Nature Research reporting summaries, source data, statements of data availability and associated accession codes are available at https://doi.org/10.1038/s41586-018-0520-5.

Received: 31 July 2017; Accepted: 23 July 2018;
Published online 12 September 2018.

1. Schneider, D. M., Nelson, A. & Mooney, R. A synaptic and circuit basis for corollary discharge in the auditory cortex. *Nature* **513**, 189–194 (2014).
2. Weiss, C., Herwig, A. & Schütz-Bosbach, S. The self in action effects: selective attenuation of self-generated sounds. *Cognition* **121**, 207–218 (2011).
3. Kuchibhotla, K. V. et al. Parallel processing by cortical inhibition enables context-dependent behavior. *Nat. Neurosci.* **20**, 62–71 (2017).
4. Zhou, M. et al. Scaling down of balanced excitation and inhibition by active behavioral states in auditory cortex. *Nat. Neurosci.* **17**, 841–850 (2014).
5. Rummell, B. P., Klee, J. L. & Sigurdsson, T. Attenuation of responses to self-generated sounds in auditory cortical neurons. *J. Neurosci.* **36**, 12010–12026 (2016).
6. Flinker, A. et al. Single-trial speech suppression of auditory cortex activity in humans. *J. Neurosci.* **30**, 16643–16650 (2010).

7. Eliades, S. J. & Wang, X. Sensory-motor interaction in the primate auditory cortex during self-initiated vocalizations. *J. Neurophysiol.* **89**, 2194–2207 (2003).
8. Singla, S., Dempsey, C., Warren, R., Enikolopov, A. G. & Sawtell, N. B. A cerebellum-like circuit in the auditory system cancels responses to self-generated sounds. *Nat. Neurosci.* **20**, 943–950 (2017).
9. Curio, G., Neuloh, G., Numminen, J., Jousmäki, V. & Hari, R. Speaking modifies voice-evoked activity in the human auditory cortex. *Hum. Brain Mapp.* **9**, 183–191 (2000).
10. Keller, G. B. & Hahnloser, R. H. R. Neural processing of auditory feedback during vocal practice in a songbird. *Nature* **457**, 187–190 (2009).
11. Eliades, S. J. & Wang, X. Neural substrates of vocalization feedback monitoring in primate auditory cortex. *Nature* **453**, 1102–1106 (2008).
12. Houde, J. F. & Jordan, M. I. Sensorimotor adaptation in speech production. *Science* **279**, 1213–1216 (1998).
13. Mifsud, N. G. & Whitford, T. J. Sensory attenuation of self-initiated sounds maps onto habitual associations between motor action and sound. *Neuropsychologia* **103**, 38–43 (2017).
14. Moore, A. K. & Wehr, M. Parvalbumin-expressing inhibitory interneurons in auditory cortex are well-tuned for frequency. *J. Neurosci.* **33**, 13713–13723 (2013).
15. Fino, E. & Yuste, R. Dense inhibitory connectivity in neocortex. *Neuron* **69**, 1188–1203 (2011).
16. Znamenskiy, P. et al. Functional selectivity and specific connectivity of inhibitory neurons in primary visual cortex. Preprint at https://www.biorxiv.org/content/early/2018/04/04/294835 (2018).
17. Williamson, R. S., Hancock, K. E., Shinn-Cunningham, B. G. & Polley, D. B. Locomotion and task demands differentially modulate thalamic audiovisual processing during active search. *Curr. Biol.* **25**, 1885–1891 (2015).
18. Nelson, A. et al. A circuit for motor cortical modulation of auditory cortical activity. *J. Neurosci.* **33**, 14342–14353 (2013).
19. Nelson, A. & Mooney, R. The basal forebrain and motor cortex provide convergent yet distinct movement-related inputs to the auditory cortex. *Neuron* **90**, 635–648 (2016).
20. Wilson, N. R., Runyan, C. A., Wang, F. L. & Sur, M. Division and subtraction by distinct cortical inhibitory networks *in vivo*. *Nature* **488**, 343–348 (2012).
21. Wolpert, D. M., Ghahramani, Z. & Jordan, M. I. An internal model for sensorimotor integration. *Science* **269**, 1880–1882 (1995).
22. Keller, G. B., Bonhoeffer, T. & Hübener, M. Sensorimotor mismatch signals in primary visual cortex of the behaving mouse. *Neuron* **74**, 809–815 (2012).
23. Froemke, R. C., Merzenich, M. M. & Schreiner, C. E. A synaptic memory trace for cortical receptive field plasticity. *Nature* **450**, 425–429 (2007).
24. Froemke, R. C. et al. Long-term modification of cortical synapses improves sensory perception. *Nat. Neurosci.* **16**, 79–88 (2013).
25. McGinley, M. J., David, S. V. & McCormick, D. A. Cortical membrane potential signature of optimal states for sensory signal detection. *Neuron* **87**, 179–192 (2015).
26. Leinweber, M., Ward, D. R., Sobczak, J. M., Attinger, A. & Keller, G. B. A sensorimotor circuit in mouse cortex for visual flow predictions. *Neuron* **95**, 1420–1432.e5 (2017).
27. Franklin, K. B. & Paxinos, G. *The Mouse Brain in Stereotaxic Coordinates, Compact. The Coronal Plates and Diagrams* (Elsevier, Amsterdam, 2008).

Acknowledgements We thank K. Tschida, M. Tanaka, and D. Purves for their comments on this manuscript; members of the Mooney laboratory for discussions regarding experimental design and data analysis; J. Pearson for comments regarding statistical analyses; and M. Booze for animal care and technical support. This research was supported by an HHMI fellowship of the Helen Hay Whitney Foundation and a Career Award at the Scientific Interface from the Burroughs Wellcome Fund (D.M.S.), the Holland-Trice Graduate Fellowship in Brain Sciences (J.S.), and NIH grant 5 R01 DC013826 (R.M.).

Reviewer information *Nature* thanks S. Eliades, G. Keller and the other anonymous reviewer(s) for their contribution to the peer review of this work.

Author contributions D.M.S., J.S., and R.M. initiated the project and designed the experiments. D.M.S. designed the aVR system, performed electrophysiology, optogenetic and calcium imaging experiments, and helped to design the psychophysics platform. J.S. designed the psychophysics platform, and performed psychophysics, pharmacology and optogenetic behavioural experiments. D.M.S. and J.S. analysed the data. D.M.S., J.S. and R.M. prepared the manuscript.

Competing interests The authors declare no competing interests.

Additional information
Extended data is available for this paper at https://doi.org/10.1038/s41586-018-0520-5.
Supplementary information is available for this paper at https://doi.org/10.1038/s41586-018-0520-5.
Reprints and permissions information is available at http://www.nature.com/reprints.
Correspondence and requests for materials should be addressed to R.M.
Publisher's note: Springer Nature remains neutral with regard to jurisdictional claims in published maps and institutional affiliations.

METHODS

Surgical procedures. All experimental protocols were approved by Duke University Institutional Animal Care and Use Committee. Male and female mice (*Mus musculus*) were purchased from Jackson Labs and were housed and bred in an onsite vivarium. We used mice that were 2–4 months old for our experiments. During all experiments, mice were kept on a reverse day–night cycle (12 h day, 12 h night).

For all surgical procedures, mice were anaesthetized under isoflurane (1–2% in O_2) and placed in a stereotaxic holder (Leica), skin was removed over the top of the head, and a titanium headpost was attached to the skull using a transparent adhesive (Metabond). Prior to electrophysiology experiments and following aVR acclimation, in male and female mice (C57, *VGAT::ChR2*, *PV::Cre*, *SST::Cre*), craniotomies were made to expose auditory cortex, auditory thalamus, and/or motor cortex to allow electrophysiology or electrical stimulation. A small craniotomy was made over the right sensory cortex and a silver pellet was positioned atop the cortical surface and cemented in place (Metabond) for use as a ground electrode. Exposed craniotomies were covered with a silicone elastomer (Kwik-Sil) and the mouse was allowed to recover in its home cage.

Prior to calcium imaging experiments, an AAV encoding Cre-dependent GCaMP6f was injected into the auditory cortex of *CaMKII::Cre* mice (see Viral injections), a tattoo was placed on the surface of the skull to mark the injection site, and a custom Y-shaped titanium headpost was attached to the skull with Metabond. Exposed skull on the top and side was also covered in Metabond. Mice were allowed to recover in their home cage for three weeks, after which time mice were again anaesthetized and a rectangular craniotomy was made over the original injection site. A stack of two laminated glass coverslips was placed over the craniotomy and sealed with Metabond. Mice were returned to their home cage and allowed to recover for 1 to 2 days.

For simultaneous psychophysics and pharmacological manipulations or optogenetic stimulation experiments (M2 terminals or $VGAT^+$ neurons) in the auditory cortex, a custom Y-shaped titanium headpost was attached to the skull with Metabond and marks were bilaterally placed on the surface of the skull over the auditory cortex. For experiments in which M2 axon terminals were activated optogenetically, an AAV encoding either Channelrhodopsin or eGFP was injected bilaterally into M2 at the same time as the headpost implant (see Viral injections). Once mice were proficient with the task, they were anaesthetized again under isoflurane and craniotomies were opened bilaterally over the auditory cortex, which was confirmed by recordings (Carbostar-1, Kation Scientific) performed at multiple locations within the craniotomy in anaesthetized mice to ensure auditory responses to 8-kHz tones (1–2 s inter-tone interval). For pharmacological experiments, exposed craniotomies were covered with a silicone elastomer (Kwik-Sil) and mice were allowed to recover in their home cage for a day before behavioural testing. For optogenetic stimulation experiments, circular glass coverslips (3 mm diameter) were implanted bilaterally over the auditory cortex and were sealed in place with Metabond. For simultaneous psychophysics and optogenetic manipulation experiments in the visual cortex ($VGAT^+$), circular glass coverslips were bilaterally implanted over visual cortex (identified using stereotaxic coordinates) at the same time as an annular headpost was attached to the skull. Mice were returned to their home cage and allowed to recover for 1 to 2 days after implantation.

Viral injections. For expression of calcium indicators, the skull over the auditory cortex of male and female *CaMKII::Cre* mice was exposed and two small craniotomies were made over the auditory cortical surface (estimated using stereotaxic coordinates) separated by approximately 300 μm along the rostral–caudal dimension. A pipette was backfilled with AAV.1.hSyn.FLEX.GCaMP6f, angled at 30° relative to vertical, and lowered into the auditory cortex. Approximately 150–200 nl virus was pressure injected (Nanoject) into the centre of auditory cortex over the course of 15 min, repeated for each craniotomy. For expression of Channelrhodopsin or eGFP, the skull over M2 of C57, or auditory cortex for *PV::Cre* and *SST::Cre* male and female mice, was exposed. A single craniotomy was made over M2 or auditory cortex (stereotaxic coordinates), and approximately 300 nl AAV.1.hSyn.ChR2.EYFP.WPRE (M2), AAV.1.CB7.eGFP.WPRE (M2) or AAV.1.EF1α.DIO.ChR2.EYFP.WPRE (A1) was pressure injected over the course of 20 min. Following injections, craniotomies were filled with melted bone wax and the injection sites were covered in Metabond.

Acoustic virtual reality. We designed a custom acoustic virtual reality (aVR) system for yoking a series of fixed-frequency tone pips (25 ms with 5 ms cosine ramp onset and offset) to a mouse's running speed. To create the aVR system, we built a non-motorized treadmill from a 6-inch Plexiglas disk (Delvies Plastic) that was coated with a thin silicone sheet (Durometer, Marian Chicago) mounted to the post of a rotary encoder (US Digital). Output from the rotary encoder was monitored with a data acquisition card (National Instruments) connected to a computer (Dell) running custom Matlab software (Mathworks, PsychToolBox) and sampled at ~30 Hz. The computer was also connected to a sound card (RME Fireface UCX), the output of which was routed to an ultrasonic speaker (Tucker Davis Technologies) located lateral to the mouse, ~15 cm from the mouse's right ear. We recorded the noise produced by the mouse's footsteps on the treadmill and the sound of the rotating treadmill itself during running by placing an ultrasonic microphone close (~1 cm) to the mouse's ear. We measured <1 dB increase (estimated by taking the root mean square (r.m.s.) value of 5-s segments of recordings) in the noise produced when the mouse was running on the treadmill compared to rest.

To calculate the inter-tone interval, we computed a filtered version of the mouse's velocity, which was the median of the last five velocity samples. Upon every sampling period, the desired inter-tone interval was updated to be proportional to the reciprocal of the current median-filtered velocity, scaled such that the rate of tone presentations closely matched the foot step rate, which was calculated from videos of mice running on the treadmill at various speeds. At speeds greater than 30 cm/s, the inter-tone-interval saturated at 100 ms to ensure spacing between tones. For the anti-coupled version of aVR, sounds were not presented while mice were running but the total number of tones that should have been presented, and the calculated intervals between them, were stored in memory. During rest, tones were played back to the mouse with inter-tone intervals drawn from the intervals that the mouse would have heard while running until the number of resting tones equalled the number of tones that mouse should have heard while running. For the metronome aVR, sounds were presented only during running and at a fixed rate (~2/s) that was not modulated by running speed.

Mice were held in place using two clamps (Altos Photonics) that secured the arms of the headpost (see Surgical procedures). On their first day of treadmill experience, the aVR system was turned off and mice ran and rested for 2 h without hearing any tones. Beginning on the second day (referred to as day 1 of aVR experience), tones of a fixed frequency were yoked to the mouse's velocity as described above. For each mouse, the tone frequency was fixed during the first 6–9 days of aVR experience at 2, 4, 8, 16, 32, or 64 kHz. Mice were placed on the treadmill for ~2 h per day and were free to transition between periods of running and rest, which typically occurred several times during each 2-h aVR acclimation session.

Electrophysiology and aVR. Following 6–9 days of aVR acclimation, mice were positioned atop the treadmill and a 32-channel electrode (Neuronexus, 4×8 configuration) was implanted into the auditory cortex or auditory thalamus. The electrode was connected to a digitizing headstage (Intan) and electrode signals were acquired, monitored in real time, and stored for subsequent offline analysis (OpenEphys). The electrode was allowed to settle for ~30 min, during which time mice ran on the treadmill and heard tones of the reafferent frequency to which they had been acclimated. Following this initial 30 min, the frequency of the running-related tones was switched from a fixed frequency to a pseudo-random distribution comprising 2, 4, 8, 16, 32 and 64 kHz tones. In a subset of mice ($N = 4$) we also included tones spaced half an octave higher and lower than the reafferent frequency. Random-frequency tones were presented with inter-tone intervals dictated by running speed. Random-frequency tones yoked to running continued until the mouse heard 50 to 100 tones of each frequency ($n = 7$ mice, 2 to 15 min) or for 30 min ($n = 4$ mice). After this time, tones with random frequency were presented during a period of rest with inter-tone intervals drawn from the distribution that the mouse had recently heard while running. Electrode signals were filtered (300 to 5,000 Hz) and action potentials from individual neurons were sorted offline for each electrode independently based on visualization of the action potential waveform and principal component analysis of the waveform using custom Matlab software (PostHawk, D.M.S.).

Tone-evoked action potential responses were measured for each neuron at each tone frequency, independently for tones presented during running and during rest. To calculate population PSTHs, the tone-evoked response of every neuron that was responsive to a particular frequency (see Statistical Methods) was averaged independently for running and resting conditions. For each neuron we measured the response strength to each tone frequency (RS(f)) as the firing rate following tone presentation minus the baseline firing rate. To calculate locomotion-related gain, we took the ratio of RS(f) measured during rest and running (gain(f) = $\mathrm{RS}(f)_{\mathrm{run}}$/$\mathrm{RS}(f)_{\mathrm{rest}}$). To average the locomotion-related gain functions across mice acclimated to aVR producing reafferent tones of different frequencies, we aligned the gain function for each neuron to the reafferent frequency experienced by the mouse from which the neuron was recorded.

Recordings from photo-identified inhibitory neurons (pi-INs) were made in *VGAT::ChR2* mice (Jackson labs) and in *PV::Cre* and *SST::Cre* mice (Jackson labs) injected with Cre-dependent ChR2 (see Viral injections). During electrophysiology, a multi-electrode array was implanted in the auditory cortex and an optical fibre coupled to a blue laser (420 nm, Shanghai) was directed at the auditory cortical surface. Action potential responses were analysed in response to a series of 30 laser pulses (100 ms each, separated by 1 s, laser power: 15–30 mW). pi-INs were identified based on short-latency, high-reliability responses to optical stimulation (Extended Data Fig. 5). Neurons that were not classified as pi-INs in *VGAT::ChR2* mice were classified as putative excitatory neurons (put-ENs). Following aVR

experience, we presented tones while recording from pi-INs during rest to measure their frequency tuning curves. The best frequency of each neuron was computed as the frequency that drove the strongest response and was restricted to neurons that were significantly driven by tones of at least one frequency. We recorded the spontaneous activity of pi-INs as mice transitioned between periods of running and rest.

To measure the strength of the functional connection between M2 and auditory cortex neurons, we implanted a bipolar stimulating electrode into M2 and we electrically stimulated within M2 (100 μs, 300 μA) every 2 s while recording from pi-INs and put-ENs in auditory cortex. Response strength to M2 stimulation was calculated as the difference between the firing rate in a baseline window immediately preceding electrical stimulation (100-ms window) and in a brief window 13 to 40 ms after electrical stimulation. We performed a bootstrap analysis 1,000 times to compute the 95% confidence bounds of the regression lines. Effect size was computed as Cohen's f^2, which is defined as $R^2/(1-R^2)$, where R is the Pearson correlation.

To measure locomotion-related suppression across cortical layers, in a subset of mice ($N=3$) we implanted the electrode perpendicular to the surface of the auditory cortical surface. To estimate the cortical layer in which each neuron on the 4×8 electrode resided, we calculated the current-source density (CSD) triggered off of tone playback. First, we created a two-dimensional map of local-field potential (LFP, bandpass filtered to include 0.1 to 70 Hz) activity by averaging across electrode shanks that were at the same depth, and plotting the averaged activity at each depth as a function of time relative to tone onset. We then computed the CSD as the second spatial derivative of the depth-specific LFP signal. We estimated which electrodes were in cortical layer 4 based on transitions between sources and sinks in the CSD and based on latency of tone-evoked responses. We then separated our electrodes into those residing in infragranular (deeper than layer 4) and supragranular (superficial to layer 4) layers of the cortex. We subsequently analysed the tone-evoked LFP signal to measure locomotion-related suppression[4].

Calcium imaging and aVR. Three weeks after viral infection with GCaMP6f and one day after the implantation of a cranial window, mice were positioned atop the treadmill and under a resonant scanning two-photon microscope (Neurolabware) with a mode-locked titanium sapphire laser (Mai Tai DeepSee) at 920 nm (laser power levels: 50–130 mW). The microscope objective (16× 0.8 NA water immersion, Nikon) was angled at ∼35° such that imaging was performed perpendicular to the auditory cortical surface while mice were positioned on the treadmill in a normal, upright position. Prior to aVR acclimation, we monitored the locomotion-related suppression of aVR-naive mice independently at each frequency. We then chose as the reafferent frequency on subsequent days the sound frequency that had the least amount of movement-related suppression for neurons in our field of view. By using this approach, we did not bias ourselves towards sound frequencies that were already strongly suppressed. On each imaging day, mice ran on the aVR treadmill and heard fixed-frequency tones yoked to their running speed for 2 h, during which time images were not acquired. Following each 2 h aVR session, tones of random frequency (2 to 64 kHz) were presented during running (with timing yoked to the mouse's running speed) and rest (with timing chosen from the running inter-tone-intervals) during image acquisition at 15.5 Hz until mice heard at least 50 tones of each frequency, typically lasting for approximately 5 to 10 min.

GCaMP6f fluorescence images were registered to correct for movement artefact in the horizontal plane. Regions of interest (ROIs) were selected using a semi-automated identification method based on nearby correlated pixel activity (Scanbox) and by manually tracing around individual cell bodies. The calcium trace for each ROI was calculated as the mean fluorescence signal averaged across all pixels comprising the ROI minus the mean fluorescence signal in an annular region surrounding each ROI (neuropil). $\Delta F/F$ was computed as $(F(t) - F_0)/F_0$, where $F(t)$ was the raw calcium snippet surrounding a single tone presentation and F_0 was the mean baseline fluorescence of each snippet during the 0.5 s preceding tone stimulation. For each neuron, we first measured whether $\Delta F/F$ was significantly elevated following tone presentation independently at each frequency ($P<0.005$, t-test).

Population-level analysis. The calcium traces of all ROIs within an imaging session that were responsive to a particular frequency were averaged together independently for tones presented during running and during rest. Across days, the population responsive to a particular frequency did not necessarily comprise the exact same neurons. To compute the reafferent suppression index (RSI), we first calculated the difference between the tone-evoked calcium traces measured during rest and during running. From the differences measured at the reafferent frequency (α) and a frequency two octaves higher or lower (β), we calculated the RSI as $(\alpha - \beta)/(\alpha + \beta)$. We then tracked RSI as a function of day following the onset of aVR experience.

Single-neuron analysis. Using anatomical coordinates and cell-body morphology, we tracked 577 neurons (from two mice) across subsequent pairs of days. Of these 577 neurons, 241 had significant tone-evoked responses to one or more tones on one or both days. For each neuron, we estimated tuning curves during rest and during locomotion on each of the two days. We then subtracted the day 1 tuning curve from the day 2 tuning curve, independently for tuning curves measured during rest and locomotion, to determine how much the tuning curve of individual neurons changed across subsequent days of aVR experience. We averaged the change in resting and change in running tuning curves across all 241 tone-responsive neurons.

Single-frequency tone detection task. Mice were acclimated to the treadmill for 2 to 3 days then water restricted for 24 h before training. To train mice to lick in response to tone presentations, tones (25 ms long, 70 and 80 dB SPL) of a fixed frequency (8 kHz) were presented with variable inter-tone-intervals (10 to 15 s) followed by a water reward 1 s later. Licking behaviour was measured with a custom-built infrared detector located between the mouse's mouth and the water delivery spout and was sampled with a data acquisition card (NI) connected to a computer (Dell) running custom software (Matlab). Within 3 to 4 days of training, mice learned to associate the tone pips with rewards. Following this initial training phase, tones were presented at variable inter-tone intervals (8 to 15 s) and mice were required to lick within a 1 s window following tone presentation to receive a reward. To ensure that mice did not lick continuously (to maximize rewards), the inter-tone-interval was reset if the mouse licked during a varying window (5 to 8 s) before tone presentation. Tones of lower intensities (0 to 60 dB, in steps of 10 dB) were gradually introduced over the subsequent 5 days.

During testing, tones were presented using a block design where each block consisted of all tone intensities (0 to 80dB in steps of 10dB) presented in random order. To ensure that the mice were engaged in the task, blocks during which the mouse did not lick were removed from analysis. Most mice spontaneously transitioned between periods of running and rest but a subset of mice tended to either rest or run continuously throughout each session. For these mice, tones were only presented during the less explored behaviour, and this transient adjustment of the task criteria was sufficient to alter a mouse's behaviour such that they began to spontaneously transition between periods of running and resting. Mice performed an average of 215 trials per day, consisting of, on average, 170 trials during rest and 45 trials during running. To create psychometric functions for each mouse, trials were separated based on whether mice were running or resting at the time of tone presentation and trials were pooled across all testing days (12.4 ± 5.4 days). 0 dB trials were used to estimate the rate of spontaneous licking and the false alarm rate. For each intensity, hit rate was calculated as the number of correct detections divided by the total number of tone presentations at each intensity. Behavioural threshold was calculated by estimating the intensity at which performance was 50% in each condition. This value was determined by linear interpolation of surrounding intensity values. To account for differences in thresholds due to difference in false alarm rates between conditions, we removed the fraction of correct trials that could be accounted for by false alarms for each condition[28]. Not applying this correction, and estimating thresholds on our raw data did not change our results (data not shown). Following training each day, mice received 1.5 ml of water. Each mouse was weighed daily to ensure that its weight did not fall below 80% of its pre-water-restriction weight.

Two-frequency tone detection task. Training and testing methods were similar to the single-frequency version of the task, but using tones of two frequencies (4 and 16 kHz). During behavioural testing, trials were presented in a block design in which each block consisted of each frequency-intensity combination (4 and 16 kHz; 0, 30, 40, 50 and 60 dB). Following an initial phase of behavioural testing, the lickometer and water spout were removed from the treadmill and mice received aVR experience with one of the two testing frequencies for 7 days, 2 h per day. Five mice each received aVR experience with 4 kHz and 16 kHz; results were consistent regardless of the aVR frequency used (data not shown). After 7 days of aVR experience, behavioural testing was performed again for 4 to 8 days. At the beginning of each day, mice received 30 min of experience with aVR, during which time they ran and heard the reafferent frequency they were acclimated to over the previous 7 days. This brief re-exposure to aVR was followed by 30 min in their home cage without any aVR or behavioural testing. At the end of this 1-h period, we reintroduced them to the behavioural testing chamber where mice performed the behavioural task.

Optogenetic stimulation during psychophysics. Mice were first trained on the single-tone detection task as described above using a subset of intensities (0, 30, 40 and 60 dB). During behavioural testing, a blue (420 nm) laser (Shanghai) was coupled to a pair of optical fibres (Doric optical splitter), which were positioned bilaterally over the auditory cortex cranial windows. Laser pulses (25 Hz, 50% duty cycle, 15–30 mW) were presented on 50% of sound trials. Laser stimulation began 200 ms before tone presentation and continued for 1.2 s, which covered the entire response window. To accurately estimate the mouse's chance performance on optogenetic trials and to deter the mouse from using light as a cue, 50% of stimuli were laser-only trials, and a short air puff (100 ms, Picospritzer II) was directed towards the mouse's face as negative reinforcement on trials where the animal licked in response to laser-only trials.

Pharmacological manipulation during psychophysics. Mice were first trained on the single-tone detection task as described above. Following initial training, saline or muscimol (2 μg/μl, 150 nl) was bilaterally pressure injected using a Nanoject system into the auditory cortex on alternate days. Mice were allowed to return to their home cage for 30 min after injection. At the end of this period, the mice were reintroduced to the testing chamber where they performed the behavioural task.

Statistical methods. Paired and unpaired two-sided statistical tests were performed with the non-parametric Wilcoxon sign rank test and Wilcoxon rank sum test, respectively, unless otherwise stated. All error bars are s.e. unless otherwise stated. Bootstrap analyses with 1,000 repetitions were used to measure confidence intervals for linear regressions (Fig. 3g, h; Extended Data Fig. 5e–i). Shuffled analyses with 1,000 repetitions were used to estimate null distributions (Fig. 1h, j). Repeated measures two-way ANOVAS followed by post-hoc Tukey tests (where required) were used to compare psychometric curves (Fig. 4c, f, h–j; Extended Data Fig. 6e–g, i–k). ANOVA *P* values were corrected using the Holm–Bonferroni method to account for multiple comparisons (Fig. 4f, h–j; Extended Data Fig. 6j, k). In all figures and captions, *n* is the number of neurons in the data sample and *N* is the number of animals contributing data points to the distributions. No statistical methods were used to predetermine sample sizes, but our sample sizes were similar to those reported in previous publications in the field. Details regarding sample sizes, *P* values and statistical tests for individual figures panels are detailed below.

Figure 1f. Of 317 neurons ($n = 11$ mice), 120 were significantly responsive to the reafferent frequency and 248 were responsive to at least one non-reafferent frequency, calculated by comparing baseline firing rates during the 100 ms preceding tone onset to the 100 ms following tone onset ($P < 0.005$, paired *t*-test). During rest, response strength (driven minus baseline firing rates) to reafferent and non-reafferent tones were not significantly different (11.2 ± 22.3 vs. 13.1 ± 24.1 action potentials/s, $n = 120$ and 248, $P = 0.46$). During running, response strength to the reafferent tone was significantly less than the response strength to non-reafferent tones (-0.1 ± 19.9 vs. 6.3 ± 23.3 action potentials/s, $n = 120$ and 248, $P = 0.001$). For a paired, within-neuron comparison, we restricted our analysis to neurons that responded to the reafferent frequency and at least one other frequency ($n = 115$) and we averaged each neuron's response to all non-reafferent frequencies to which it responded significantly. During running, responses to the reafferent frequency were weaker than to non-reafferent frequencies ($P = 1.1 \times 10^{-18}$, Wilcoxon signed-rank test). As a population, responses to the reafferent frequency during running were not significantly different from 0 ($P = 0.12$).

Figure 1h. We aligned the gain function for each neuron to the reafferent frequency experienced by the mouse from which the neuron was recorded. The number of neurons responsive to each tone frequency (–3, –2, –1, 0, 1, 2, and 3 octaves, relative to the reafferent frequency) were 70, 92, 153, 120, 110, 95, and 67, respectively. To determine whether the notch at the reafferent frequency was significant relative to what would be expected by chance, we shuffled the data by randomly assigning to each neuron a reafferent frequency rather than using the actual frequency experienced by the mouse from which the neuron was recorded. This shuffling was performed 1,000 times and the 95% confidence bounds of the distribution were computed.

Figure 1j. As in Fig. 1h. 109 neurons were recorded from five mice. The number of neurons responsive to each tone frequency (–2, –1, 0, 1, and 2 octaves, relative to the reafferent frequency) were 24, 39, 33, 24, and 20, respectively. As in Fig. 1h, we computed confidence bounds by randomly assigning to each neuron a reafferent frequency rather than using the actual frequency experienced by the mouse from which the neuron was recorded.

Figure 2c. Solid lines show the mean calcium response to tones averaged across all neurons that were responsive to that tone during rest. The population size that was responsive to each tone on each day is noted below each set of red and black traces. Vertical line shows d*F*/*F*.

Figure 2i. For 241 neurons, the tuning curves estimated across subsequent days were subtracted, and this was done independently for curves measured during rest (black) and running (red). At each frequency (and independently for each movement condition), we performed a bootstrap analysis, randomly sampling from our distribution (with replacement), repeated 1,000 times. The shaded areas show the 95% confidence bounds for these distributions. The only significant change in tuning was at 32 kHz (the reafferent frequency) and only during locomotion (red).

Figure 3d. Data are from pi-INs recorded from two *PV::Cre* mice ($n = 36$), two *SST::Cre* mice ($n = 21$), and three *VGAT::ChR2* mice ($n = 44$). Magenta, green and black asterisks indicate $P = 0.03$, $P = 0.04$, and $P = 0.02$, respectively. Analysing all interneurons together, $P = 0.01$. (sign rank and rank sum tests for paired and unpaired tests, respectively).

Figure 3g. Data are from pi-INs recorded from two *PV::Cre* mice ($n = 54$), two *SST::Cre* mice ($n = 32$), and five *VGAT::ChR2* mice ($n = 75$). Solid lines are linear regression and shaded lines show 95% confidence bounds from a bootstrap analysis repeated 1,000 times.

Figure 3h. Data are from pi-INs recorded from two *PV::Cre* mice ($n = 33$) and two *SST::Cre* mice ($n = 26$). PV^+ and SST^+ neurons were pooled for the regression analysis. Solid lines are linear regression and shaded lines show 95% confidence bounds from a bootstrap analysis repeated 1,000 times.

Figure 3i. Data are from regressions shown in **g** and Extended Data Fig. 5g–i. Effect sizes for PV, VGAT, SST, and all pi-INs are significantly larger than effect sizes for non-reafferent and naive conditions ($P < 0.01$, Wilcoxon). Effect sizes for PV, VGAT and all pi-INs are significantly larger than effect size for put-ENs ($P < 0.01$, Wilcoxon). Bar height determined by linear fit of raw data; error bars show s.e. of linear fits from 1,000 repetitions of bootstrap analysis.

Figure 4c. Resting and running performance curves are mean and s.e. for $N = 19$ mice. Lines are sigmoid fits to the data points. Comparisons with repeated measures two-way ANOVAs at non-zero intensities (factors: intensity × behavioural state, P(interaction) = 0.0003, $F(7, 126) = 4.22$), followed by post-hoc Tukey test. Red asterisks, $P < 0.005$.

Figure 4d. Each point contains the behavioural threshold (intensity at 50% performance) during rest and running for a single mouse. Comparisons with two-sided paired *t*-test. $P = 0.009$.

Figure 4f. Data points show mean and s.e. for $N = 4$ mice. Rest versus optogenetic activation of inhibitory interneurons in the auditory cortex: comparisons with repeated measures two-way ANOVAs at non-zero intensities. (factors: intensity × laser state, P(interaction) = 0.01, $F(2, 6) = 14.27$, post-hoc Tukey test, blue asterisk $P < 0.05$). Rest versus running: comparisons with repeated measures two-way ANOVAs at non-zero intensities (factors: intensity × behavioural state, P(interaction) = 0.03, $F(2, 6) = 6.60$, post-hoc Tukey test, red asterisk $P < 0.05$). ANOVA *P* values were corrected using the Holm–Bonferroni method.

Figure 4h. Data points show mean and s.e. for $N = 4$ mice. Rest versus optogenetic activation of M2 axon terminals in the auditory cortex: comparisons with repeated measures two-way ANOVAs at non-zero intensities (factors: intensity × laser state, P(interaction) = 0.04, $F(2, 6) = 5.84$, post-hoc Tukey test, blue asterisk, $P < 0.05$). Rest versus running: comparisons with repeated measures two-way ANOVAs at non-zero intensities. (factors: intensity × behavioural state, P(interaction) = 0.04, $F(2, 6) = 8.29$, post-hoc Tukey test, red asterisk, $P < 0.05$). ANOVA *P* values were corrected using the Holm–Bonferroni method.

Figure 4i. Data points show mean and s.e. for $N = 10$ mice during rest and running. Comparisons in each subpanel with repeated measures two-way ANOVAs at non-zero intensities (factors: intensity × behavioural state. For tone A: P(interaction) = 0.0002, $F(3, 27) = 11.56$. For tone B: P(interaction) = 0.04, $F(3, 27) = 3.85$), followed by post-hoc Tukey test. ANOVA *P* values corrected using the Holm–Bonferroni method. Red asterisks, $P < 0.05$.

Figure 4j. Data points show mean and s.e. for $N = 10$ mice during rest and running. Comparisons with repeated measures two-way ANOVAs at non-zero intensities (factors: intensity × behavioural state. For tone A: P(interaction) = 0.01, $F(3, 27) = 5.62$. For tone B: P(interaction) = 0.05, $F(3, 27) = 2.90$), followed by post-hoc Tukey test. ANOVA *P* values were corrected using the Holm–Bonferroni method. Red asterisks, $P < 0.05$.

Reporting summary. Further information on experimental design is available in the Nature Research Reporting Summary linked to this paper.

Data availability. The data that support the findings of this study are available from the corresponding author upon reasonable request.

28. Glickfeld, L. L., Histed, M. H. & Maunsell, J. H. Mouse primary visual cortex is used to detect both orientation and contrast changes. *J. Neurosci.* **33**, 19416–19422 (2013).

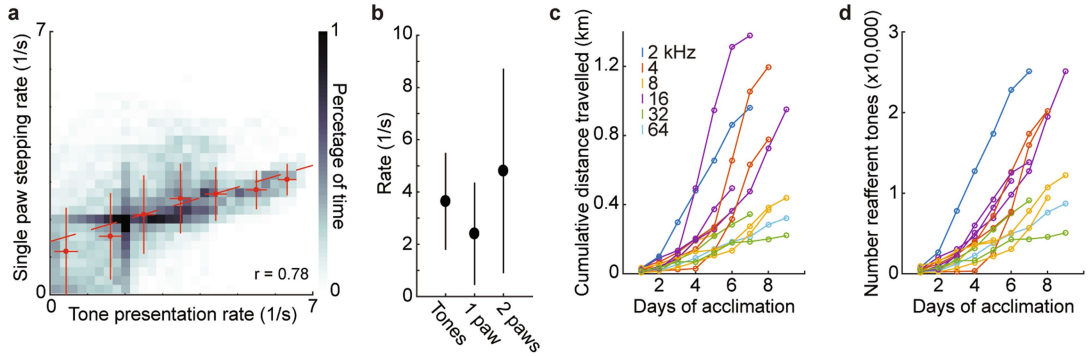

Extended Data Fig. 1 | aVR experience is coupled to locomotion. **a**, Heat map showing the rate of tone presentation as a function of instantaneous stepping rate with a single paw, measured via simultaneous videography. Data points show mean ± s.d. tone rate and stepping rate in 1-Hz (1 s^{-1}) bins. Red dashed line shows linear regression through all data points. Reafferent tones during aVR experience were strongly correlated to instantaneous paw stepping rate (0.78). Data are from 3,716 steps recorded from 1,804 s of video from two mice. **b**, Average tone presentation rate during aVR experience closely matches average stepping rate measured either with a single paw or two paws. Dots are median and error bars are s.d. **c**, Cumulative distance run by 11 mice over 6–9 days of aVR experience. Each line is for a different mouse, colour-coded by the reafferent frequency to which the mouse was acclimated. **d**, Cumulative number of tones heard by same 11 mice as in **c**.

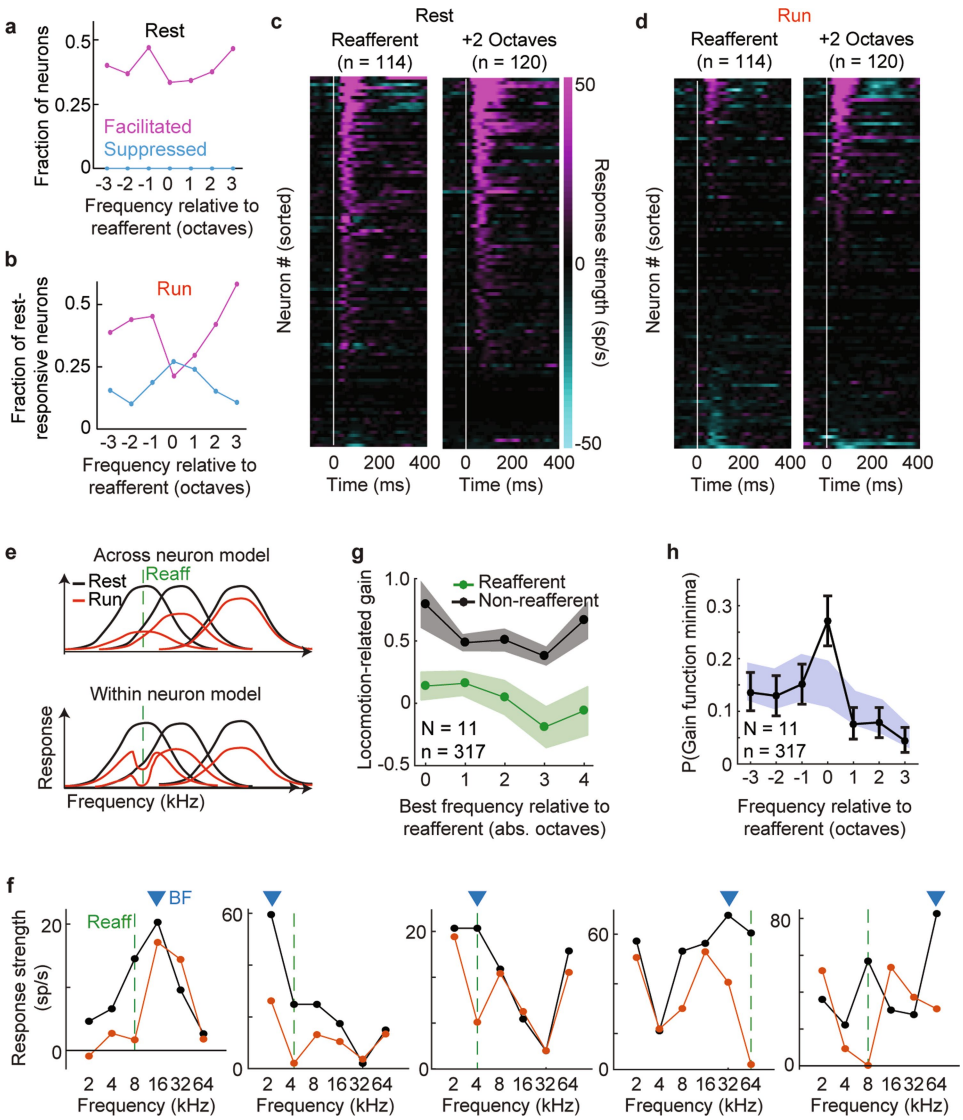

Extended Data Fig. 2 | aVR experience alters locomotion-related suppression at the level of individual neurons. a, Fraction of neurons with elevated firing rates (magenta) and suppressed firing rates (cyan) in response to tones during rest. A roughly equal number of neurons were excited by the reafferent frequency as were excited by other frequencies. **b**, Fraction of rest-responsive neurons with elevated firing rates (magenta) and suppressed firing rates (cyan) in response to tones of varying frequency during running. Nearly 50% of neurons were responsive to non-reafferent frequencies during running, whereas fewer than 25% were responsive to the reafferent frequency. **c**, Heat map showing response strength (tone-evoked rate – baseline rate) for neurons responsive to the expected reafferent frequency (left, $n = 114$ neurons, $N = 11$ mice) and another frequency (+2 octaves, $n = 120$ neurons, $N = 11$ mice) during rest. Neurons ordered by magnitude of response independently for each heat map. **d**, Response strengths of the neurons in **c** during running. Neurons are re-sorted by magnitude of response. Twenty-three per cent of neurons retained their response to the reafferent frequency during running, consistent with a sparse representation of expected reafferent sounds. **e**, Two alternative models for how locomotion-related suppression could change following aVR experience. In each model, the black curves show frequency tuning curves of three neurons during rest, red curves during running, and the green dashed line indicates the reafferent frequency. Across-neuron model: locomotion-related suppression is uniform across frequencies within a neuron but is strongest for neurons that are strongly responsive to the expected reafferent frequency. Within-neuron model: suppression is non-uniform at the single neuron level and regardless of how strongly the neuron responds to the expected reafferent frequency, suppression is always strongest at the reafferent frequency. **f**, Tuning curves for five example neurons measured during rest (black) and running (red). The best frequency (BF) for each neuron is shown by the blue triangle, and the reafferent frequency to which each mouse was acclimated is shown by the green dashed line. In all five neurons, locomotion-related suppression was strong at the reafferent frequency relative to other frequencies, regardless of the neuron's best frequency. **g**, Neurons were sorted by their best frequency, measured relative to the reafferent frequency that each mouse experienced. Locomotion-related suppression at the expected reafferent frequency (green) and averaged across all non-reafferent frequencies (black). Regardless of a neuron's best frequency, suppression was always strongest at the reafferent frequency, supporting the within-neuron model in **e**. Sample size: $N = 11$ mice, $n = 314$ neurons. Shaded regions show 95% confidence bounds estimated with a bootstrap analysis repeated 1,000 times. **h**, Probability of observing a minima in the gain function of individual neurons at each frequency, measured relative to the reafferent frequency. A substantial number of neurons had minima in their gain functions at the expected reafferent frequency, further supporting the within-neuron model in **e**. Sample size: $N = 11$ mice, $n = 314$ neurons. Shaded region shows a null distribution, which we estimated by randomly assigning to each neuron a reafferent frequency rather than using the actual frequency experienced by the mouse from which the neuron was recorded. This shuffling was performed 1,000 times and the 95% confidence bounds of the distribution were computed. Error bars show the 95% confidence bounds estimated from a bootstrap analysis repeated 1,000 times.

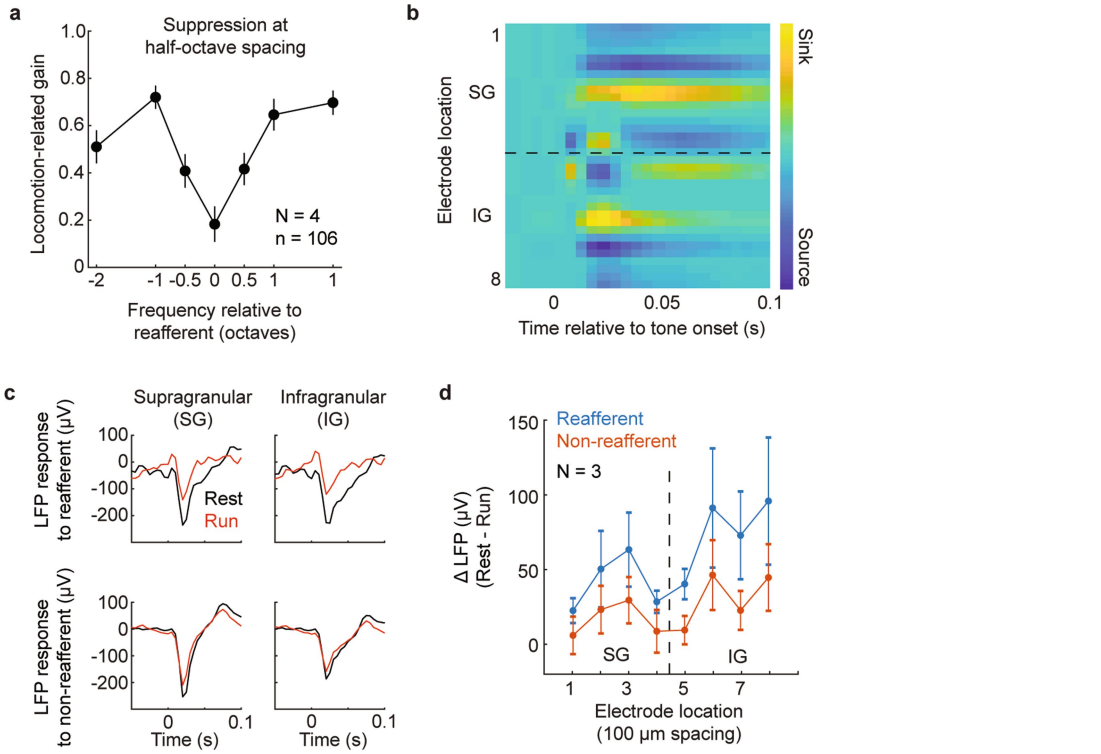

Extended Data Fig. 3 | Specificity of suppression following aVR experience. a, Locomotion-related gain tested at half-octave spacing from the reafferent frequency. Neuronal responses to frequencies half an octave from the reafferent frequency were suppressed at an intermediate level. Data are mean ± s.e. Sample size: $N = 4$ mice, $n = 106$ neurons. **b**, Example current-source density triggered by tone-onset for electrode recordings made perpendicular to the auditory cortical surface. Black dashed line demarcates putative supragranular (SG) and infragranular (IG) layers of cortex. Electrode 1 is the most superficial; electrode spacing is 100 μm. **c**, Example tone-evoked local field potential (LFP) traces from an SG electrode (left) and an IG electrode (right) in response to the expected reafferent frequency (left) and a non-reafferent frequency (right). Locomotion-related suppression of LFP responses was stronger for the reafferent frequency than for non-reafferent frequencies. Data are mean ± s.e. **d**, The difference in LFP between rest and running as a function of electrode location (1 is the most superficial; electrode spacing is 100 μm; $N = 3$ mice). Positive values indicate greater suppression during locomotion.

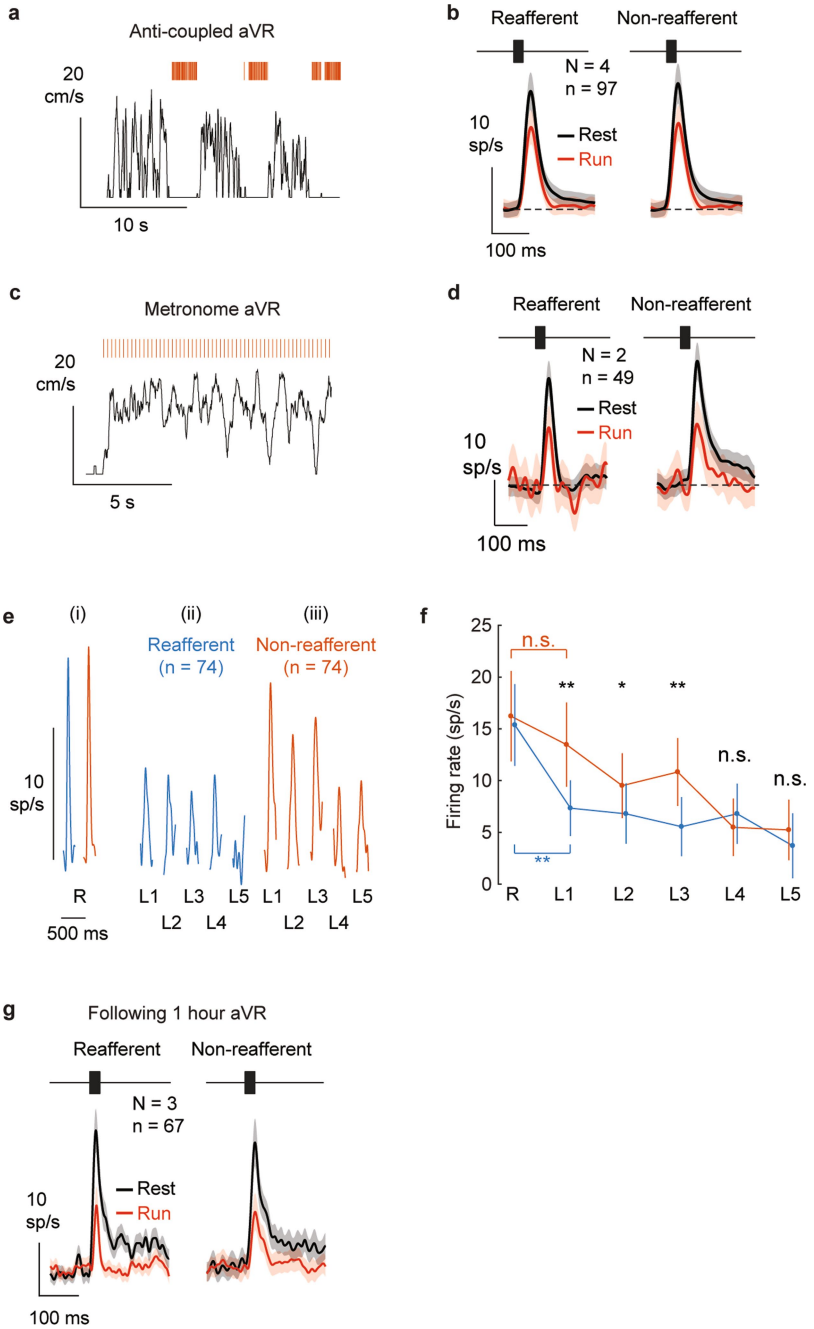

Extended Data Fig. 4 | See next page for caption.

Extended Data Fig. 4 | Frequency-specific locomotion-related suppression requires several days of coupled sensory–motor experience. a, Example sensory–motor experience during anti-coupled aVR experience. Mice did not hear tones while running, but tones were played back during subsequent resting periods with inter-tone intervals drawn from the intervals that mice should have heard while running. **b**, Population PSTHs for the expected frequency (left) and for non-reafferent frequencies (right) during rest (black) and running (red) following anti-coupled aVR. Anti-coupled aVR experience does not lead to changes in auditory responsiveness during running or rest. Sample size: $N = 4$ mice, $n = 97$ neurons. Shaded region shows mean ± s.e. $P = 0.57$, two-sided Wilcoxon rank sum test. **c**, Example sensory–motor experience during metronome aVR experience. Tones were presented during running at a fixed rate (2 s^{-1}) but the tone rate was not modulated by running speed. **d**, Population PSTHs for the expected frequency (left) and for non-reafferent frequencies (right) during rest (black) and running (red) following metronome aVR. Metronome aVR experience does not lead to changes in auditory responsiveness during running or rest. Sample size: $N = 2$ mice, $n = 49$ neurons. Shaded region shows mean ± s.e. $P = 0.57$, two-sided Wilcoxon rank sum test. **e**, Mice were acclimated to aVR for 7 days. On the day of electrophysiology, we altered on each locomotor bout the sound produced by the treadmill to be either expected (blue) or a non-reafferent frequency (2 octaves away, red). We then analysed responses ($N = 4$ mice, $n = 74$ neurons) to each sound frequency during rest (R) and to the first five tones heard at the beginning of each bout of locomotion (L1–L5). (i) Tone-evoked responses (population PSTHs) to the reafferent (blue) and a non-reafferent sound (red) during rest. (ii) Tone-evoked responses during locomotion to the first five tones in a series of the expected reafferent frequency. (iii) Tone-evoked responses during locomotion to the first five tones heard in a series of non-reafferent tones. **f**, Firing rates to the reafferent (blue) and non-reafferent (red) reafferent sounds during rest (R) and during the first five tones heard during locomotion (L1–L5). Responses to the first tone heard during locomotion were significantly suppressed only if that tone matched the expected reafferent frequency (blue asterisk, $P = 0.002$, two-sided Wilcoxon signed rank test). Black asterisks indicate significant differences between firing rates to the reafferent and non-reafferent reafferent sounds (L1, $P = 0.002$; L2, $P = 0.03$; L3, $P = 0.007$, two-sided Wilcoxon rank sum test). Sample size: $N = 4$ mice, $n = 74$ neurons. Red n.s. indicates that evoked responses to the first tone heard during a bout of running are not significantly different from those evoked during rest for non-reafferent tones ($P = 0.4$, two-sided Wilcoxon signed rank test). **g**, Population PSTHs for the expected frequency (left) and for non-reafferent frequencies (right) during rest (black) and running (red). Data were collected from three mice ($n = 67$ neurons) after each mouse's first experience of hearing fixed-frequency reafferent tones for 1 h, during which time mice heard 927, 3,167 and 1,069 reafferent tones at 16 kHz, 2 kHz and 16 kHz, respectively. This experience was insufficient to shift the locomotion-related suppression towards the reafferent frequency. Shaded region shows mean ± s.e. $P = 0.47$, two-sided Wilcoxon rank sum test.

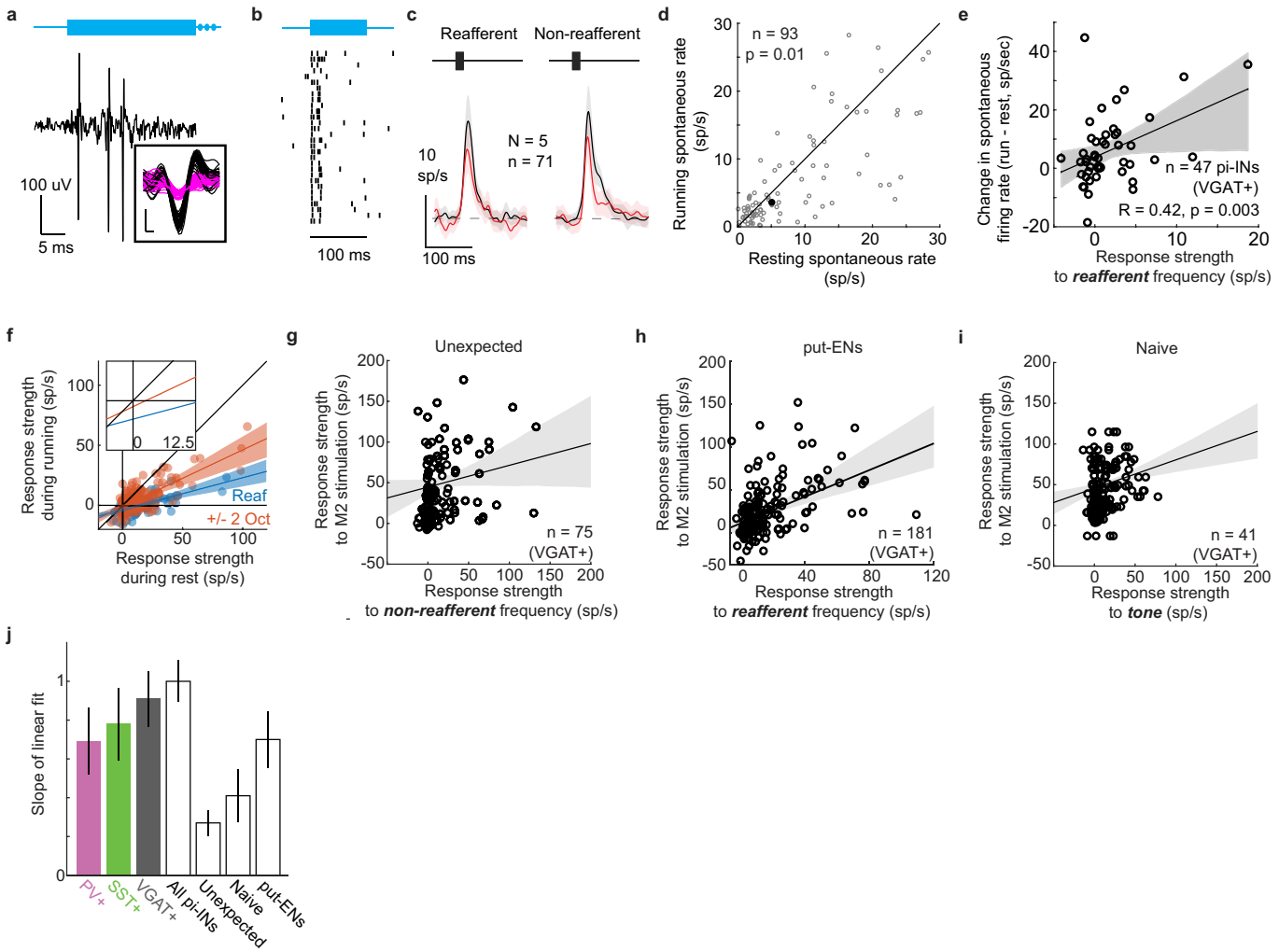

Extended Data Fig. 5 | Characterizing photo-identified inhibitory neurons in auditory cortex. a, Voltage trace of a pi-IN recorded from a *VGAT::ChR2* mouse in response to a 100-ms pulse of blue light targeted to the cortical surface. Inset shows example waveforms belonging to the sorted unit (black) and belonging to the noise cluster (magenta), showing good electrophysiological isolation. **b**, Rasters showing response of the same neuron to 30 pulses of blue light (100 ms each). **c**, Tone-evoked responses of auditory cortical inhibitory neurons ($VGAT^+$) during rest (black) and locomotion (red) in response to reafferent (left) and non-reafferent (right) frequencies. Responses are suppressed during locomotion, but suppression is not specific to the reafferent frequency. Sample size: $N = 5$ mice, $n = 71$ neurons. Shaded region shows mean ± s.e. $P = 0.36$, two-sided Wilcoxon rank sum test. **d**, Spontaneous firing rate during rest and locomotion for 93 putative excitatory neurons (non-photo-identified in *VGAT::ChR2* mice, $N = 7$ mice). Filled circle shows mean. Firing rates were significantly lower during running relative to rest (two-sided Wilcoxon signed rank test). **e**, pi-INs ($VGAT^+$) that were more strongly driven by the reafferent frequency were more strongly recruited during running. $N = 2$ mice, $n = 47$ neurons. Black line and shaded area show linear regression and 95% confidence bounds from a bootstrap analysis repeated 1,000 times, respectively. The P value represents the probability that the slope of the regression line includes zero, estimated from the bootstrap analysis. **f**, Tone-evoked responses during running and rest for the reafferent frequency (blue) and non-reafferent frequencies (±2 octaves, red). Dots are responses of individual neurons ($N = 11$ mice, $n = 317$), lines are linear regression, and shaded regions are 95% confidence bounds from bootstrap analysis repeated 1,000 times. Suppression to non-reafferent sounds is best fit as a gain model (slope = 0.47 ± 0.05; offset = –0.19 ± 0.70), whereas suppression of expected reafferent tones has a stronger gain component (that is, shallower slope, two-sided Wilcoxon rank sum test, $P = 3.3 \times 10^{-317}$) and an offset term that is significantly different from zero (slope = 0.27 ± 0.4; offset = –3.55 ± 0.58. two-sided signed rank test, $P = 3.3 \times 10^{-165}$). Inset shows a zoom in of the regression lines near the origin. These data suggest that suppression of expected reafferent sounds involves both divisive and subtractive forms of inhibition. **g**, Responses to a non-reafferent tone in $VGAT^+$ pi-INs recorded from aVR-acclimated mice were weakly correlated with responses to electrical stimulation in M2 ($n = 75$ neurons from 5 mice). These data indicate that the strong relationship between tone-evoked responses and M2 stimulation responses in auditory cortical pi-INs is distinct to the reafferent frequency. Black line and shaded area show linear regression and 95% confidence bounds from a bootstrap analysis repeated 1,000 times, respectively. **h**, Responses to the expected reafferent tone in put-ENs recorded from aVR-acclimated mice were correlated with responses to electrical stimulation in M2 ($n = 181$ neurons from 5 *VGAT::ChR2* mice). This effect size for put-ENs is significantly weaker than for pi-INs. Black line and shaded area show linear regression and 95% confidence bounds from a bootstrap analysis repeated 1,000 times, respectively. **I**, Responses to a non-reafferent tone in $VGAT^+$ pi-INs recorded from naive mice were weakly correlated with responses to electrical stimulation in M2 ($n = 41$ neurons from 2 mice). Black line and shaded area show linear regression and 95% confidence bounds from a bootstrap analysis repeated 1,000 times, respectively. **j**, Slope of the linear fit for the relationship shown in Fig. 3i. Error bars show 95% confidence bounds from a bootstrap analysis. Data are from regressions shown in Fig. 3g and Extended Data Fig. 5g–i. Slopes of linear fit for PV, VGAT, SST, and all pi-INs are significantly larger than slopes of linear fits for non-reafferent and naive conditions ($P < 0.01$, Wilcoxon). Bar height determined by linear fit of raw data; error bars show s.e. of linear fits from 1,000 repetitions of bootstrap analysis.

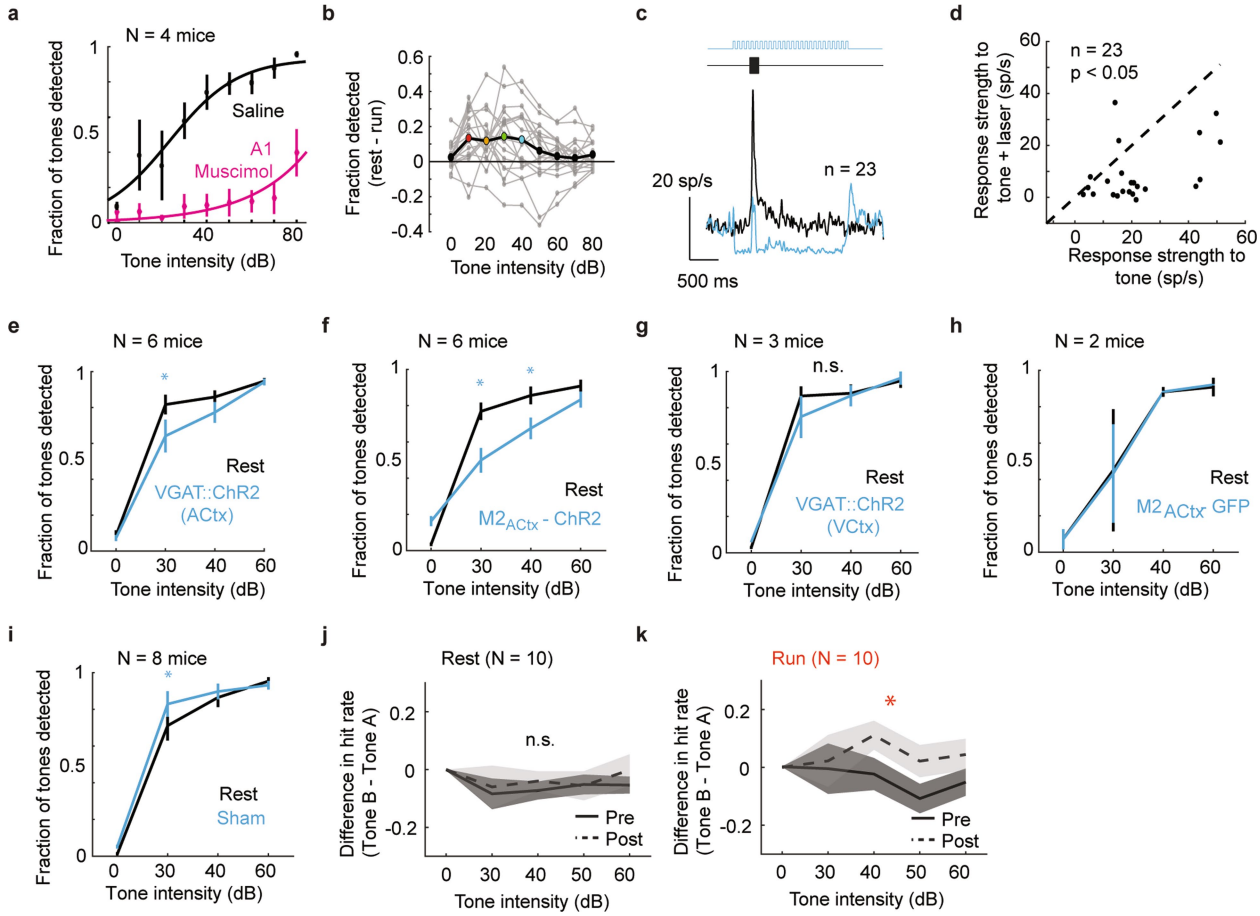

Extended Data Fig. 6 | Tone detection behaviour is compromised by locomotion, is auditory-cortex dependent, and adapts following VR experience. a, Data points show mean and s.e. detection rates for $N = 4$ mice as a function of tone intensity for trials performed during rest with infusion of either saline (black) or muscimol (magenta) into the auditory cortex. **b**, Difference in performance as a function of intensity for each mouse (grey dots). Large connected dots show mean difference in performance and coloured dots indicate intensities at which performance was significantly different ($P < 0.05$) across conditions ($N = 19$ mice, repeated measures two-way ANOVA followed by post-hoc Tukey test). **c**, Tone-evoked responses from putative excitatory neurons recorded from *VGAT::ChR2* mouse without (black) and with (blue) simultaneous blue laser stimulation. Optogenetic activation of inhibitory neurons decreases the spontaneous and tone-evoked firing rates of excitatory neurons. $n = 23$ neurons, $N = 1$ mouse. **d**, Tone-evoked firing rates during rest are weaker during optogenetic activation of inhibitory interneurons. Dashed line is unity. ($n = 23$ neurons, $N = 1$ mouse; $P < 0.05$, two-sided paired t-test.) **e**, Tone detection performance ($N = 6$ mice) during rest (black) and rest with optogenetic activation of auditory cortical inhibitory neurons (blue). Mice were worse at detecting tones on optogenetic trials (repeated measures two-way ANOVA, factors: intensity × laser state, P(intensity × laser state) = 0.0028, $F(2, 10) = 11.23$, post-hoc Tukey test at individual intensities, blue asterisk, $P < 0.05$ on laser trials) compared to rest. **f**, Tone detection performance ($N = 6$ mice) during rest (black) and rest with optogenetic activation of M2 terminals in auditory cortex (blue). Four of these mice were presented with 8-kHz tones and the remaining two were presented with 4-kHz tones. Mice were worse at detecting tones on optogenetic trials regardless of the tone frequency. (Statistics similar to **e**, P(intensity × laser state) = 0.01, $F(2, 10) = 6.66$, blue asterisk, $P < 0.05$ on laser trials). **g**, Average psychometric functions ($N = 3$ mice) showing detection rates as a function of tone intensity for trials performed during rest when visual cortex was inhibited. (repeated measures two-way ANOVA, P(intensity × laser state) = 0.33, $F(2, 4) = 1.47$). **h**, Average psychometric functions ($N = 2$ mice) showing detection rates as a function of tone intensity for trials performed during rest (black) and during rest with laser stimulation (blue) by mice injected with an AAV encoding eGFP in M2. These controls show that laser stimulation of auditory cortex in the absence of ChR2 does not influence behaviour. **i**, Average psychometric functions ($N = 8$ mice) showing detection rates as a function of tone intensity for trials performed during rest (black) and during rest with laser stimulation (blue) when the optical fibre was placed over intact skull near, but not directly over auditory cortex. Five of eight mice were injected with an AAV encoding ChR2 into M2, of which three were presented with 8-kHz tones and 2 with 4-kHz tones. The other three were *VGAT::ChR2* mice presented with 8-kHz tones. These controls show that sham laser stimulation (which is visible to the mouse) alone improves behaviour (repeated measures two-way ANOVA, factors: intensity × laser state, P(interaction) = 0.0066, $F(2, 14) = 7.35$, post-hoc Tukey tests, blue asterisk, $P < 0.05$). **j**, Difference in hit rates in response to tone A relative to tone B during rest before (pre) and after (post) aVR experience with tone A.). Lines represent mean difference and shaded regions show s.e. for $N = 10$ mice. There is no difference in rest performance before and after aVR experience. (repeated measures two-way ANOVA in each panel, factors: intensity × time of testing, P(time of testing) = 0.46, $F(1, 9) = 0.61$). **k**, Difference in hit rates in response to tone A relative to tone B during running before (pre) and after (post) aVR experience with tone A. Lines represent mean difference and shaded regions show s.e. for $N = 10$ mice. Mice are significantly better at detecting tone B than tone A after aVR experience, indicating that this is a movement-specific change (repeated measures two-way ANOVA in each panel, factors: intensity × time of testing, P(time of testing) = 0.04, $F(1, 9) = 8.07$, red asterisk, $P < 0.05$, p values in **j**, **k** corrected using the Holm–Bonferroni method. For further statistical details, see Supplementary Table 1.

nature research

Corresponding author(s): Richard Mooney, Ph.D.

Reporting Summary

Nature Research wishes to improve the reproducibility of the work that we publish. This form provides structure for consistency and transparency in reporting. For further information on Nature Research policies, see Authors & Referees and the Editorial Policy Checklist.

Statistical parameters

When statistical analyses are reported, confirm that the following items are present in the relevant location (e.g. figure legend, table legend, main text, or Methods section).

n/a	Confirmed	
☐	☒	The exact sample size (*n*) for each experimental group/condition, given as a discrete number and unit of measurement
☐	☒	An indication of whether measurements were taken from distinct samples or whether the same sample was measured repeatedly
☐	☒	The statistical test(s) used AND whether they are one- or two-sided *Only common tests should be described solely by name; describe more complex techniques in the Methods section.*
☐	☒	A description of all covariates tested
☐	☒	A description of any assumptions or corrections, such as tests of normality and adjustment for multiple comparisons
☐	☒	A full description of the statistics including central tendency (e.g. means) or other basic estimates (e.g. regression coefficient) AND variation (e.g. standard deviation) or associated estimates of uncertainty (e.g. confidence intervals)
☐	☒	For null hypothesis testing, the test statistic (e.g. *F*, *t*, *r*) with confidence intervals, effect sizes, degrees of freedom and *P* value noted *Give P values as exact values whenever suitable.*
☒	☐	For Bayesian analysis, information on the choice of priors and Markov chain Monte Carlo settings
☒	☐	For hierarchical and complex designs, identification of the appropriate level for tests and full reporting of outcomes
☐	☒	Estimates of effect sizes (e.g. Cohen's *d*, Pearson's *r*), indicating how they were calculated
☐	☒	Clearly defined error bars *State explicitly what error bars represent (e.g. SD, SE, CI)*

Our web collection on statistics for biologists may be useful.

Software and code

Policy information about availability of computer code

Data collection	ScanBox (version 2.5); OpenEphys (Gui version 0.3.5); Matlab (2013b,2014a); PsychToolBox (version 3.0.12)
Data analysis	ScanBox (version 2.5); Matlab (R2016a, 2016b); Graphpad Prism (version 7.0.3)

For manuscripts utilizing custom algorithms or software that are central to the research but not yet described in published literature, software must be made available to editors/reviewers upon request. We strongly encourage code deposition in a community repository (e.g. GitHub). See the Nature Research guidelines for submitting code & software for further information.

Data

Policy information about availability of data

All manuscripts must include a data availability statement. This statement should provide the following information, where applicable:

- Accession codes, unique identifiers, or web links for publicly available datasets
- A list of figures that have associated raw data
- A description of any restrictions on data availability

Custom code used and datasets generated and/or analyzed during the current study are available from the corresponding author upon reasonable request.

Field-specific reporting

Please select the best fit for your research. If you are not sure, read the appropriate sections before making your selection.

☒ Life sciences ☐ Behavioural & social sciences ☐ Ecological, evolutionary & environmental sciences

For a reference copy of the document with all sections, see nature.com/authors/policies/ReportingSummary-flat.pdf

Life sciences study design

All studies must disclose on these points even when the disclosure is negative.

Sample size	No statistical methods were used to pre-determine sample sizes, but our sample sizes were similar to those reported in previous publications in the field.
Data exclusions	No data were excluded in these studies.
Replication	All attempts at replication were successful. The results are based on behavior and recordings from multiple mice and multiple neurons (as described in the text) and the reproducibility of the findings are shown in the scatter plots and other accompanying figures.
Randomization	Our study did not contain experimental groups so randomization does not apply.
Blinding	Our study did not contain experimental groups so blinding does not apply,

Reporting for specific materials, systems and methods

Materials & experimental systems

n/a	Involved in the study
☒	☐ Unique biological materials
☒	☐ Antibodies
☒	☐ Eukaryotic cell lines
☒	☐ Palaeontology
☐	☒ Animals and other organisms
☒	☐ Human research participants

Methods

n/a	Involved in the study
☒	☐ ChIP-seq
☒	☐ Flow cytometry
☒	☐ MRI-based neuroimaging

Animals and other organisms

Policy information about studies involving animals; ARRIVE guidelines recommended for reporting animal research

Laboratory animals	Our study used male and female mice (C57, VGAT::ChR2, PV::Cre, SST::Cre), 2-4 months old.
Wild animals	Our study did not involve any wild animals.
Field-collected samples	Our study did not involve any field-collected samples.